Indian Journal of Engineering & Materials Sciences
Vol. 10, October 2003, pp. 341-352

Analysis of non-reacting flow in an aircraft gas turbine engine afterburner model using finite volume method

M Rajkumar & V Ganesan

Internal Combustion Engines Laboratory, Department of Mechanical Engineering,
Indian Institute of Technology Madras, Chennai 600 036, India

Received 17 February 2003; accepted 11 July 2003

This paper focuses on the aerodynamics of the non-reacting flow inside an aero-gas turbine engine afterburner by carrying out a three-dimensional CFD analysis using the finite volume approach. A 60° sector of the afterburner with all the complexities has been modelled to take advantage of the symmetry of the design. The computational methodology employed SIMPLE algorithm for pressure velocity coupling, RNG k–ε model for turbulence in an unstructured and non-uniform grid. The analysis has been carried out for sea level inlet conditions. A recirculation zone was seen to be formed behind the V-gutters and inner wall of the diffuser. The performance of the diffuser was found to be good and the Mach number just upstream of the V-gutter was found to be in line with requirements. The pressure loss was in line with successful designs and the nozzle performance was found to be satisfactory. The predicted flow fields are verified using existing experimental results. The results for various mass flow rates and different geometries are presented for the closed nozzle position.

Military turbojets require greater thrust during take off and high speed 'dogfight' manoeuvers. Various methods of thrust augmentation exist and the principle is to either increase the mass flow rate (by injection of water, water alcohol mixture or refrigerants), or increase the energy (by burning fuel in the turbine exhaust or air bled from compressor). The constraining factor being space and weight, as also the cost, the afterburner has become the universal choice for military turbojets. It fits into the tailpipe region and has the most favourable thrust to weight ratio.

But the afterburner also entails some penalty in the form of pressure losses (cold loss) when it is not in use as also the 'hot losses' when in use. The components required for achieving the design intent in an afterburner also cause unavoidable pressure losses in the turbojet. A diffuser is provided at the turbine exit in order to decelerate the flow so as to allow combustion to initiate. Flame stabilizer is provided in order to ensure that proper combustion takes place and blowout of flame does not take place. The fuel manifolds are provided to supply the fuel into the combustion chamber. Supporting structures also cause obstruction in the flow and cause pressure losses.

Thus the afterburner contributes not only to additional length and weight, but also introduces unavoidable pressure and thrust losses. Modernday afterburners are invariably the bypass type. Introduction of bypass flow to cater to anti-screech and liner cooling requirements further complicates the geometry. The mass flow from bypass and the resulting mixing needs to be analyzed in order to achieve the desired results, viz., proper cooling of the liner, screech suppression and combustion. The flow inside the afterburner is complex and thereby the performance of the afterburner would depend almost entirely on aerodynamics. Therefore, it becomes necessary to study the aerodynamics of flow in the afterburner so as to optimize the design for the conflicting requirements of short usage and relatively longer non-usage. Further analysis of reacting flow can be considered with a geometrically optimized afterburner.

Owing to the complexity involved, experimental investigations are costly, time-consuming and accessible only to government funded laboratories. The advent of numerical methods and commercially available codes, along with declining cost of computing power has made it possible for such flow fields to be analyzed at a fraction of the cost of experimental investigations. It also allows for geometry optimization and generation of flow fields for various conditions.

Useller *et al.*[1] presented the results of several full-scale turbojet-engine afterburner investigations

conducted by erstwhile NACA. Various combustion chamber lengths were evaluated considering the combustion efficiency as the criterion of afterburner performance. Edwards[2] summarized much of the early development work and designs. He has reported on the high frequency, high amplitude form of combustion instability called screech, which caused mechanical failures in practical engines. Kumar[3] has proposed a method for estimating pressure loss across flame holders in high velocity streams. A simple relationship relating the flame holder blockage and the gutter-included angle gave a reasonably good prediction of total pressure loss. Over the range tested it was found that loss coefficients are nearly independent of the Reynolds number. Ganesan[4] has predicted the turbulent flow behind a conical baffle using finite difference prediction procedure. The flow was assumed to be 2D axisymmetric, steady, turbulent and non-reacting. Governing differential equations, together with boundary conditions were solved by finite difference method based on SIMPLE algorithm. Axial and radial velocities along with turbulent kinetic energy behind the bluff body were predicted at various axial locations for a particular inlet velocity.

Ravichandran and Ganesan[5] conducted an experimental investigation of the three-dimensional confined flow fields behind a typical afterburner flame stabilizer. The flame stabilizer comprised of one main ring V-gutter with twelve outer and six inner radial V-gutters, concentrically placed within a cylindrical pipe. Recirculation zones were captured behind each of the above. The three mean velocity components were determined using a five-hole pitot probe measurements along the entire length of the cylinder, which was considered for experimentation in three different azimuthal planes. The computer prediction codes and the development of turbulence models for simulation find a much-needed database with the help of the time-mean velocity measurements. Lee and Lin[6] conducted numerical simulation of non-reacting flows of a two-ring flame stabilizer using a zonal grid method. They demonstrated that zonal grid method is a useful approach for simulating complex geometry of flame holder flows. SIMPLE type calculation procedure in a boundary fitted coordinate system with a non-staggered grid arrangement and standard κ-ε turbulence model were employed in the simulation. In the computation of flow of the two-ring flame holder, change in the flow pattern was observed by staggering the flame holders. However, the overall length of the re-circulation zone remained essentially the same. Ravichandran and Ganesan[7] conducted detailed three-dimensional analysis of isothermal flow in an afterburner using finite volume formulation. Calculations were performed using SIMPLE algorithm with non-staggered grid arrangement. Turbulence was modelled using the κ-ε model. The geometry consisted of an annular diffuser, V-gutter flame stabilizer with radial as well as ring gutters and a variable area nozzle. The results showed acceleration between two ring gutters, producing re-circulation zones behind them, the lower one being lengthy due to the combined effect of the diffuser. The sharp angled cropped diffuser produced better mixing near the bottom ring than near the top ring.

The predicted flow fields in the absence of the radial gutter confirmed that the radial gutters are the chief source of generation of swirl momentum near the flame stabilizer. Predictions without the diffuser indicate that the top re-circulation zone will be longer than the bottom. Predictions for various inlet swirl ratios and inlet axial velocity profiles show the potential usefulness of the method to designers. Frovlov *et al.*[8] presented a mathematical approach for studying bluff body flame stabilization in confined flows with open boundaries. The approach is based on the Favre averaged conservation laws, a standard κ-ε model for turbulence, presumed probability density function closure for the mean reaction rate and 'non-reflecting' boundaries at open boundaries. The bluff bodies considered included V-gutter, plates and cylinders. Temperature fields in a combustor showed that the most stable flame is provided by the V-gutter. The examination of the velocity profiles indicated that the flame stability is directly related to the maximum velocity, which is maximum for the cylinder and minimum for the V-gutter. Ravichandran and Ganesan[9] performed experimental and numerical investigations of the three-dimensional flow fields in an isothermal model of an afterburner consisting of a typical turbofan afterburner flame stabilizer. The measurements indicated the formation of individual re-circulation regions behind ring, inner and outer gutters in different azimuthal planes. The length of re-circulation region behind the outer gutter was found to be more than that of the inner gutter and which provided a long shear layer through which burnt and unburnt products exchanged producing high levels of turbulent mixing to stabilize the flame. The numerical

calculations were performed using a SIMPLE based algorithm with staggered grid arrangement and standard κ-ε model was used for physical modelling. The identification of flow regions with pronounced three dimensionalities or established cyclic behaviour provided useful information for the improvement of numerical modelling exercises, viz., choice of turbulence models and use of zonal approach for the complex geometries.

Ravichandran and Ganesan[10] presented a computational study of the three-dimensional flow field development, chemical reaction and combustion processes in a typical afterburner system under both isothermal and reacting flow conditions. The calculations were based upon a numerical solution of the time-averaged transport equations for mass, momentum, turbulence kinetic energy, dissipation rate, enthalpy and species concentrations using a finite-volume formulation. The physical models included the κ-ε turbulence model, the eddy break-up model, a two-step reaction model, a droplet vapourization and combustion model and six-flux radiation model. The predicted reacting flow parameters identified a number of design parameters such as fuel injector location, high degree reaction zone, nozzle opening area and the corresponding fuel flow rate.

Mathematical Modelling

The four fundamental physical equations, viz., the equation of state, the equation of continuity, the equations of momentum in three directions and the energy equation can express any general flow problem. The solution of these fundamental equations with the proper boundary conditions generates 'solution' of the flow. Computational methods are useful in discretising these equations in the domain of interest and allow us to use one of the many numerical methods to arrive at acceptable 'solution'. The 'solution' provides us a comprehensive insight into the complex flow phenomenon, which is beyond the scope of experimental investigation.

The time averaged governing equations for fluid flow in the Cartesian tensor form are as follows:

Continuity equation

$$\frac{\partial}{\partial X_i}(\rho u_i)=S_m \qquad \ldots (1)$$

where u_i is the mean velocity component and S_m the source term, which accounts for the mass added due to the vapourization of liquid droplets, and is zero in the case of non-reacting flow. (For the purpose of non-reacting analysis, combustion is not considered).

Momentum equation in the X-direction

$$\frac{\partial}{\partial X_j}(\rho u_i u_j)=-\frac{\partial p}{\partial X_i}+\frac{\partial}{\partial X_j}\left[\mu\left(\frac{\partial u_i}{\partial X_j}+\frac{\partial u_j}{\partial X_i}-\frac{2}{3}\delta_{ij}\frac{\partial u_i}{\partial X_i}\right)\right]+\frac{\partial}{\partial X_j}(-\rho\overline{u_i' u_j'})+F_i \qquad \ldots (2)$$

where p is the static pressure, μ the molecular viscosity, δ_{ij} is the kronecker-delta function and F_i the external body force that arises from the interaction with the dispersed phase in the i direction. The second term on the right hand side represents the stress tensor denoted by τ_{ij}. The third term on the right hand side of the above equation represents the Reynolds' stresses and these are modelled using the Boussinessq hypothesis. According to this hypothesis the Reynolds' stresses are related to the mean velocity gradients by:

$$-\rho\overline{u_i' u_j'}=\mu_t\left(\frac{\partial u_i}{\partial X_j}+\frac{\partial u_j}{\partial X_i}\right)-\frac{2}{3}\left(\rho k+\mu_t\frac{\partial u_i}{\partial X_i}\right)\delta_{ij} \qquad \ldots (3)$$

where k is the turbulent kinetic energy and μ_t is turbulent viscosity whose computational method depends on the type of turbulence model used.

Energy equation

In the present case due to the mixing of the colder bypass flow with the hotter core flow results in mixing regions which affect the flow field and hence the energy equations needs to be solved. The heat transfer has however, been ignored. The heat added due to chemical reactions has not been considered.

$$\frac{\partial}{\partial X_i}(u_i(\rho E+p))=\frac{\partial}{\partial X_i}\left(k_{eff}\frac{\partial T}{\partial X_i}-\sum_j h_j j_j+u_j(\tau_{ij})_{eff}\right)+S_H \qquad \ldots (4)$$

where k_{eff} is the effective thermal conductivity ($k_l + k_t$, k_t is the turbulent thermal conductivity), and J_j is the diffusion flux of the species j. S_H is the heat added due to the chemical reaction.

In the above equation:

$$E = h - \frac{p}{\rho} + \frac{u_i^2}{2} \quad \ldots (5)$$

Turbulence modelling

The random nature of a turbulent flow precludes computations based on a complete description of the motion of all the particles. A turbulence model is a computational procedure to close the system of mean flow equations, which contain unknowns (Reynolds' stresses) as a result of the time averaging operation done on the momentum equations. The computational procedure should be able to predict these unknowns with reasonable accuracy. The two equation k-ε classical model has been used to model the turbulence. Specifically the RNG variant of the equation is used. The RNG variant is derived from the instantaneous Navier-Stokes equations, using a mathematical technique called the "renormalization group" method. It is similar in form to the standard k-ε model, but includes some refinements, which make the model more accurate and reliable for a wider class of flows compared to the standard k-ε model.

The transport equation for turbulent kinetic energy k and its dissipation rate ε are obtained from the following transport equations:

$$\rho \frac{Dk}{Dt} = \frac{\partial}{\partial X_i}\left[\alpha_\varepsilon \mu_{eff} \frac{\partial k}{\partial X_i}\right] + G_k - \rho\varepsilon - Y_M \quad \ldots (6)$$

and

$$\rho \frac{D\varepsilon}{Dt} = \frac{\partial}{\partial X_i}\left[\alpha_\varepsilon \mu_{eff} \frac{\partial \varepsilon}{\partial X_i}\right] + C_{1\varepsilon}\frac{\varepsilon}{k} G_k - C_{2\varepsilon}\rho\frac{\varepsilon^2}{k} - R \quad \ldots (7)$$

In the above equations G_k represents the generation of turbulent kinetic energy due to the mean velocity gradients and is evaluated as follows:

$$G_k = 2\mu_t S_{ij} S_{ji} \quad \ldots (8)$$

where the mean strain rate S_{ij} is given by:

$$S_{ij} = \frac{1}{2}\left(\frac{\partial u_i}{\partial X_j} + \frac{\partial u_j}{\partial X_i}\right) \quad \ldots (9)$$

$C_{1\varepsilon}$, $C_{2\varepsilon}$ are the model constants having the following default values derived analytically by the RNG theory:

$C_{1\varepsilon} = 1.42$, $C_{2\varepsilon} = 1.68$.

The quantities α_k and α_ε are the inverse effective Prandtl numbers for k and ε respectively which are computed using the following formula derived from the RNG theory:

$$\left|\frac{\alpha - 1.3939}{\alpha_0 - 1.3929}\right|^{0.6321} \left|\frac{\alpha + 2.3929}{\alpha_0 - 2.3929}\right|^{0.3679} = \frac{\mu_{mol}}{\mu_{eff}} \quad \ldots (10)$$

where $\alpha_0 = 1.0$ obtained from the contribution of fluctuating component in compressible turbulence. For high Reynolds number turbulent flow, the value of $\alpha_k = \alpha_\varepsilon$ is taken to be 1.393.

Y_M represents dissipation rate and is calculated by:

$$Y_M = 2\rho\varepsilon\left(\frac{k}{a^2}\right) \quad \ldots (11)$$

where a represents sonic velocity.

The R term in Eq.(7) marks the difference in ε equation between the RNG and standard k-ε model and it accounts for the effects of rapid strain. It is given by:

$$R = \frac{C_\mu \rho \eta^3 \left(1 - \frac{\eta}{\eta_0}\right)}{1 + \beta\eta^3} \frac{\varepsilon^2}{k} \quad \ldots (12)$$

where $\eta \equiv Sk/\varepsilon$, $\eta_0 = 4.38$, $\beta = 0.012$.

S is the scalar measure of the deformation tensor and is given by:

$$S \equiv \sqrt{2\Omega_{ij}\Omega_{ji}} \quad \ldots (13)$$

where Ω_{ij} is the mean rate of rotation tensor and is defined by:

$$\Omega_{ij} = \frac{1}{2}\left(\frac{\partial u_j}{\partial X_i} - \frac{\partial u_i}{\partial X_j}\right) \quad \ldots (14)$$

The scale elimination procedure in RNG theory results in a differential equation for turbulent viscosity:

$$d\left(\frac{\rho^2 k}{\sqrt{\varepsilon\mu}}\right)=1.72\frac{(\mu_{eff}/\mu)}{\sqrt{(\mu_{eff}/\mu)^3-1+C_\upsilon}}\times d(\mu_{eff}/\mu) \quad \ldots (15)$$

where $C_\upsilon \approx 100$.

Eq.(15) is integrated to obtain an accurate description of how effective turbulent transport varies with the effective Reynolds number. However in the high Reynolds-number limit, Eq. (15) gives:

$$\mu_t=\rho C_\mu \frac{k^2}{\varepsilon} \quad \ldots (16)$$

with C_μ =0.0845 derived using the RNG theory. In the present study turbulent viscosity has been evaluated from Eq. (16). The above sets of equations are solved by the finite volume method[8] using the commercially available FLUENT[9] 6 code.

Afterburner Configuration

Afterburner is designed as an extension that can fit into the tailpipe region. It is located between turbine and exhaust nozzle. Fig. 1 shows a schematic of a turbojet engine with an afterburner. The schematic shows a gas generator with twin spool arrangement.

The primary combustor is located between the compressor and the turbine stages and the exhaust from the low-pressure turbine is made to pass through the afterburner before exiting through the nozzle. It can be seen from the figure that the engine dimensions dictate the radial dimensions of the afterburner.

A 60° sector of the afterburner is shown in Fig. 2 and a brief description of the components is given below.

Diffuser

The gas velocity after the turbine is high and would cause blowout of flame in case combustion is attempted. Hence, the gas has to be decelerated to initiate and sustain combustion. The diffuser is a diverging duct in which the flow velocity is brought down from Mach 0.4-0.5 to about Mach 0.25-0.3. It also incorporates some de-swirling struts to ensure that the swirl present in the flow after the turbine does not cause blowout of the flame.

Fuel manifolds

The gas from the turbine contains enough oxygen and hence, fuel alone needs to be injected. The injection is achieved by the fuel manifolds, which ensure an even distribution of fuel with sufficient velocity and pressure to cause atomization and proper mixing.

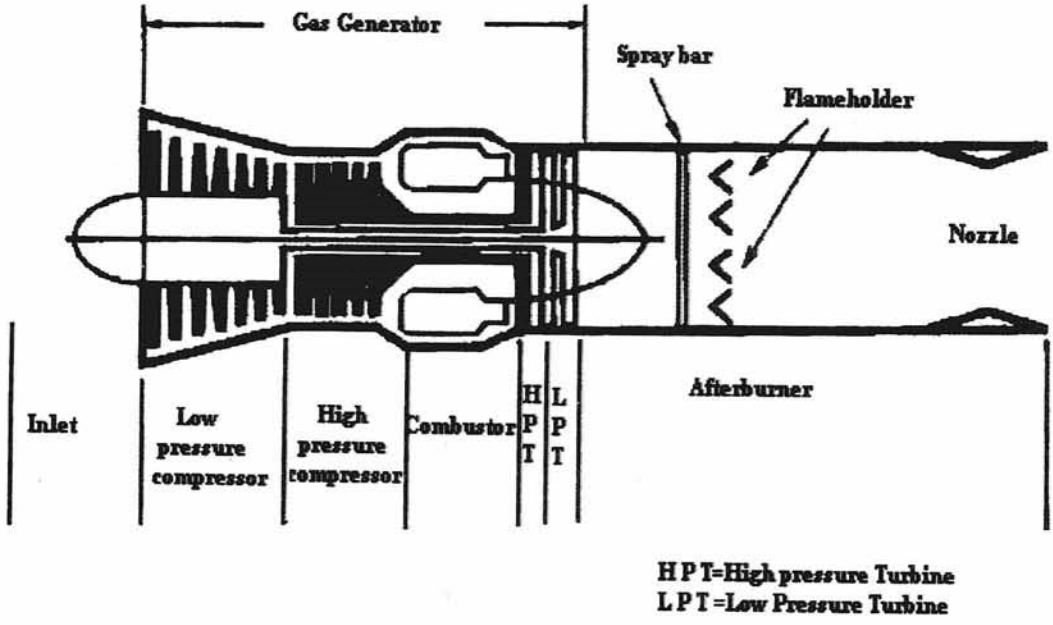

Fig. 1—Schematic of turbojet engine with afterburner

Flame stabilizer (V-Gutter)

It is known that in high speed flows combustion cannot be sustained and flame suffers from 'blowout'. In order to initiate, and sustain combustion in such flows, it is necessary to introduce a flame-holder/ flame stabilizer or a bluff body. The flame stabilizer creates a recirculation zone immediately downstream, wherein the fuel and oxidizer enjoy sufficient residence time and the velocities are low. This is a zone of low reaction rates, near stoichiometric conditions and almost adiabatic flame temperature. The fuel particles constantly get trapped into this recirculation zone and thus provide a constant source of ignition. This zone of turbulence interacts with the flow field and creates 'mixing zones' which are characterized by very high turbulence dissipation rates, high rates of energy and species transfer resulting in rapid reaction rates. This 'constant source of ignition' ensures that the flame is sustained and given sufficient length, the fuel is completely combusted.

Anti-screech liner

High speed combustion causes combustion related instabilities in the form of pressure fluctuations which not only create the 'jet screech' but also has the potential to extinguish the flame. The modern day afterburners provide a perforated annulus that damps the fluctuations.

Cooling rings

The combustion in afterburner produces very high wall temperatures that could cause failure of the liner wall. To prevent such a failure, cooling rings with holes provide entrance to the bypass air that acts as jet pipe liner-cooling air and ensure that the liner temperature is well below the critical limit.

Nozzle

Flow velocity is enhanced in this section. In afterburners the nozzle is convergent-divergent type since the gas velocity at inlet usually approaches about Mach 0.7. Due to this reason even in the non-afterburning condition a divergent section is required. The throat area of the nozzle can be varied depending on the mode of operation, viz., afterburning or non-afterburning. The nozzle opening and closing is coupled with fuel supply through a fuel-scheduling program so that the nozzle is correctly matched at all operation points.

Casing

It is a structural shell, which carries thrust loads and houses all the components of the afterburner along with the bypass duct, which receives air bled from the compressor.

Geometric Modelling

In the present study the dimensions of a typical afterburner have been taken up for the geometric modelling and grid generation using GAMBIT pre-processor. The actual geometry is quite complex and modelling the exact geometry with all the geometric

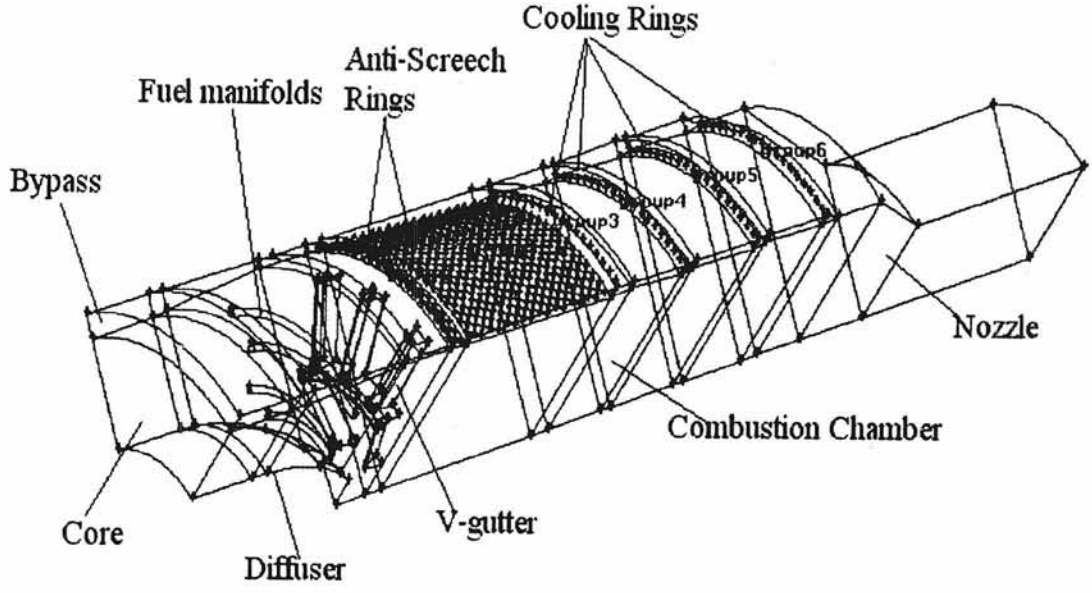

Fig. 2— 60° sector of the afterburner

details would require an extremely fine mesh size to capture all the details and compute and therefore geometric details that do not affect the flow field significantly have been neglected. Shorn of such geometric details, only a 60° sector (Fig. 2) of the total configuration has been modelled so as to exploit the symmetry. The nozzle is in the closed (non-afterburning) position. Fig. 3 gives a magnified view of the flame stabilizer. The V-gutter shown in Fig. 3 has 18 top radial gutters and 6 bottom radial gutters with the ring gutter bridging the gap between them. The top and bottom radial gutters are positioned at an angle of 20° to the vertical and the included angle of the V in all the gutters is 30°.

Unstructured grid with tetrahedral cells has been used for discretising the computational domain. Non-uniform meshing has been adopted so as to provide a fine mesh near the flame stabilizer where large gradients in flow variables are expected. A relatively coarser mesh has been adopted in the region comprising of the nozzle and tail pipe where not much variation in flow is expected. The mesh size is 0.83 million.

Boundary conditions

The boundaries in the computational domain are inlet, outlet, wall and periodic/cyclic. Diffuser inner wall, bypass flow top wall, V-gutter and fuel manifolds have been specified as wall boundary condition where the particles are trapped. Mass flow inlet and pressure outlet boundary conditions have been chosen for inlet and outlet boundaries respectively. The side faces have been specified as periodic/cyclic boundary condition in order to take advantage of the symmetry of geometry as well as the flow. The core and the bypass flows are allowed to mix through the anti-screech, cooling rings and the bypass exit where interior boundary condition has been applied. The operating conditions have been chosen as sea level conditions. The fluid has been specified as compressible ideal gas. The values of the boundary conditions, thermodynamic and flow properties are tabulated in Table 1.

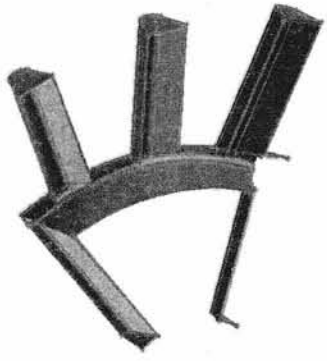

Fig. 3—Ring and radial V-gutters

Results and Discussion

The analysis has been carried out for 60° sector of the three-dimensional computational model of a typical afterburner in order to get an insight into the aerodynamics of the flow in the afterburner.

Fig. 4 shows the velocity contour plot at mid-section plane through the computational model. It is seen that the velocity decreases in the diffuser section of the afterburner and reaches a value of around 100 m/s just upstream of the V-gutter. A recirculation zone is formed immediately downstream of the V-gutter and is characterized by a region of low velocity. Subsequently the velocity remains more or less constant except in the regions where the colder bypass flow and hotter core flow mix. A sharp increase in the velocity is seen in the nozzle section

The static temperature contours are presented in Fig. 5, wherein the static temperature is more or less constant in the domain. The static temperature is seen to fall sharply in the nozzle section contributing to the velocity increase. The temperature near the liner is lower than the average temperature owing to the mixing of the two flows.

The contours of static and total pressure are presented in Figs 6 and 7 respectively. The static pressure recovery in the diffuser section can be seen as also the drop in the nozzle section due to expansion. The throat area of the nozzle is seen to cause an unsustainable sharp drop in pressure and as a result the pressure is seen to rise downstream. Further,

Table 1—Boundary condition specifications

Mass flow rate (Core inlet)	15 kg/s
Mass flow rate (Bypass inlet)	2.2 kg/s
Total temperature (Core inlet)	1050 K
Total temperature (Bypass inlet)	517 K
Turbulence intensity (Core inlet)	10%
Turbulence length scale (Core inlet)	0.0123 m
Turbulence intensity (Bypass inlet)	5%
Turbulence length scale (Bypass inlet)	0.00374 m
Gauge pressure (Outlet)	0 Pa

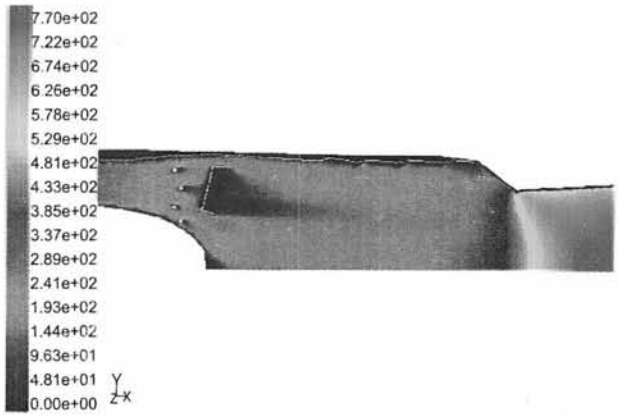

Fig. 4—Velocity (m/s) contours at mid plane

Fig. 5—Static temperature (K) contours at mid plane

Fig. 6—Static pressure (Pa) contours at mid plane

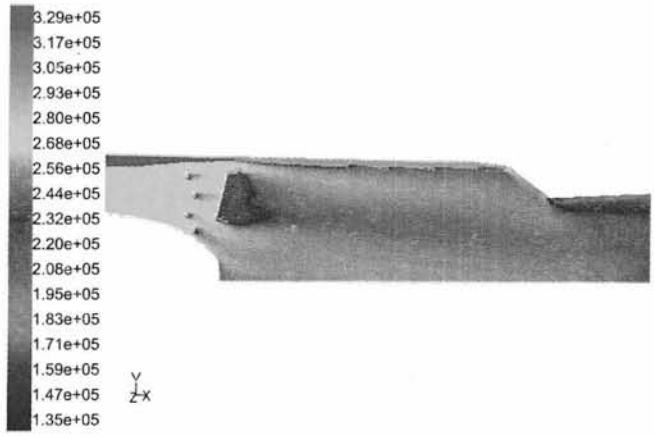

Fig. 7—Total pressure (Pa) contours at mid plane

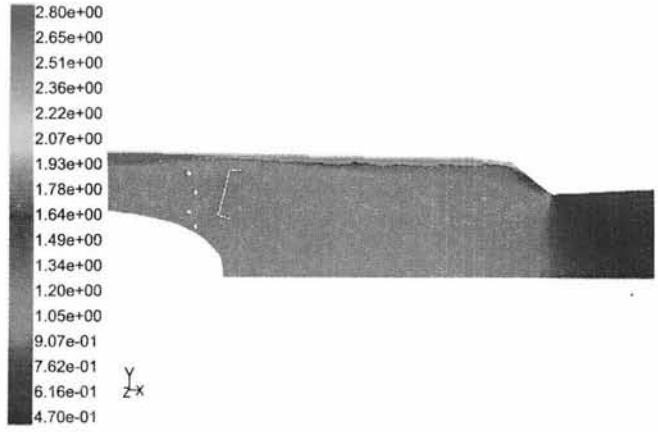

Fig. 8—Density (kg/m^3) contours at mid plane

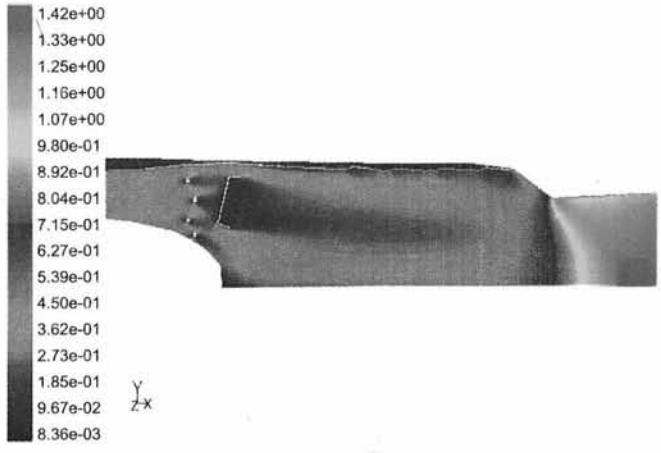

Fig. 9—Mach number contours at mid plane

downstream the pressure falls. This can be seen to be contributing to the pressure loss in Fig. 7. The other regions causing pressure loss are the V-gutter, fuel manifolds, truncated inner wall of diffuser and the mixing regions of core and bypass flows. It is suggested that the pressure loss in the throat area of the nozzle could be avoided by better design of the convergent-divergent nozzle.

Fig. 8 shows the density contours which are in line with expectations and contiguous with plots of other thermodynamic and flow properties.

Fig. 9 shows the Mach number contours at the mid plane. It is seen that the diffuser performance is satisfactory in that the Mach number just upstream of the V-gutter is reduced to about 0.28 from a value of around 0.43 at core inlet. In the nozzle section the Mach number at outlet is around 1.34. A sonic line, curved as expected, is seen to form starting from the throat area. In this figure too the deleterious effect of the improper throat design on the flow field is clearly seen. The recirculation zone at the truncated inner wall of the diffuser is seen in this figure.

The total temperature in Fig. 10 is conserved since the study is restricted to non-reacting case. The mixing of the two flows produces a region of lower temperature near the liner around 750 to 800 K.

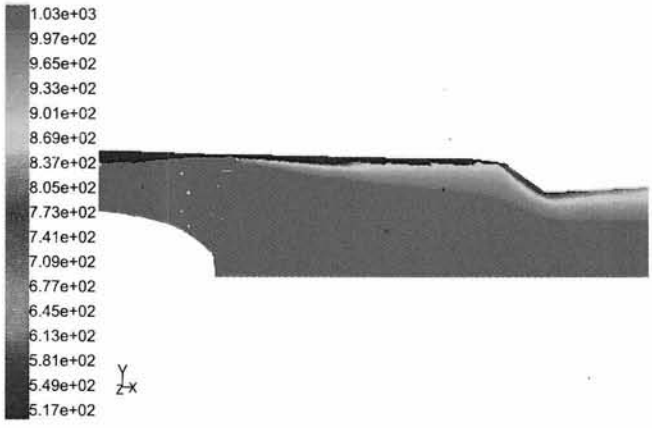

Fig. 10—Total temperature (K) contours at mid plane

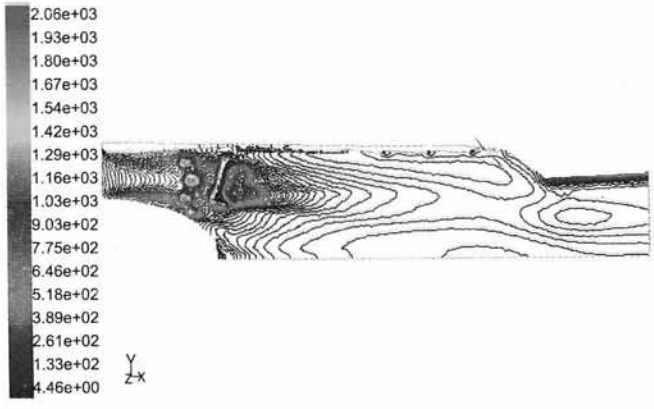

Fig. 11—Turbulence kinetic energy (m^2/s^2) contours at mid plane

The turbulence kinetic energy contours are presented at Figs 11-13 at mid plane and at planes rotated 20° and 30° about x-axis respectively. The recirculation zone is characterized by production of TKE in the lee of the V-gutter and it's high dissipation in the flow field causes shear zones that result in high reaction rates and rapid combustion. It is seen that the flow enters the domain with some TKE, which dissipates in the diffuser section itself. The presence of the fuel manifolds acts as bluff bodies and causes production of TKE. The effects of the top radial, ring and bottom radial gutters are seen clearly in Figs 11-13 respectively. The length of the recirculation zone behind the top radial gutter is seen to be longer than the bottom radial gutter and would provide longer shear layers through which diffusion of burnt and unburnt products would occur. The effect of the ring gutter is seen clearly in Fig. 12. The ring

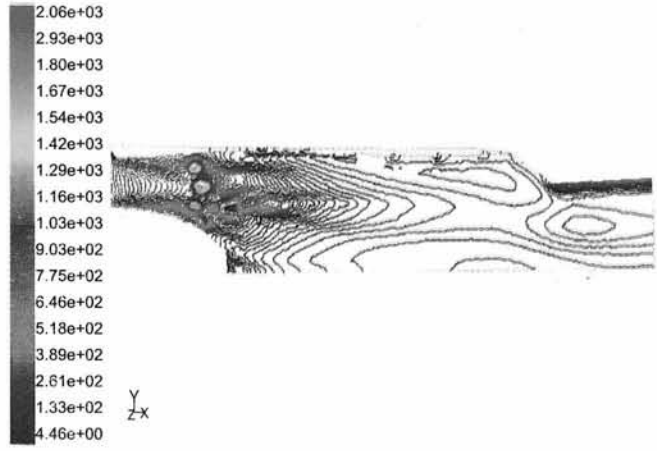

Fig. 12—Turbulence kinetic energy (m^2/s^2) contours at a plane rotated 20° about x-axis from the mid plane

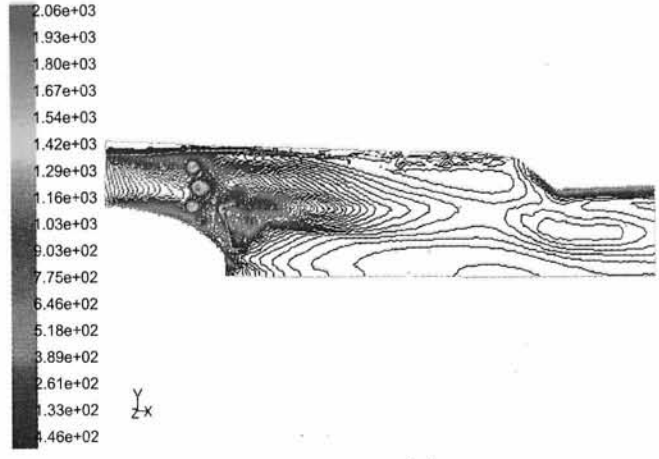

Fig. 13—Turbulence kinetic energy (m^2/s^2) contours at a plane rotated 30° about x-axis from the mid plane

gutter is seen to cause a relatively shorter recirculation zone, but the contribution to recirculation zone overall is important in that the maximum TKE occurs at regions where the radial and ring gutters meet. In these figures too the recirculation zone at the truncated inner wall of the diffuser section can be seen as also the unnecessary turbulence in the throat area of the nozzle.

Similarly the plots of velocity vectors at mid plane and at planes rotated through 20° and 30° are presented in Figs 14-16 respectively. These figures too are contiguous to the TKE contours. The recirculation zone is seen to be clearly delineated. The contribution of the ring gutter to the overall recirculation zone can be clearly seen. The vectors indicate that the particles get trapped in the lee of the ring gutter and subsequently travel upwards and downwards along the inner-shielded portion of the top and bottom radial gutters. As expected the flow then has clockwise rotation at the top section of the top radial gutter and anti-clockwise at the bottom section. The bottom radial gutter exhibits reverse characteristics for the flow rotational direction. This zone allows the flame to anchor in the high-speed flow and provides the necessary continuous ignition source for flame stabilization. Such plots could be used to determine the injection points and spray pattern for the fuel in order to take advantage of the recirculation zone and shear layers created.

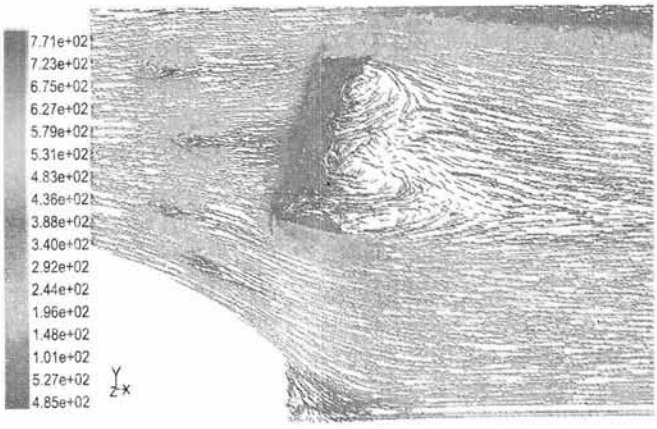

Fig. 14—Velocity (m/s) contours at mid plane

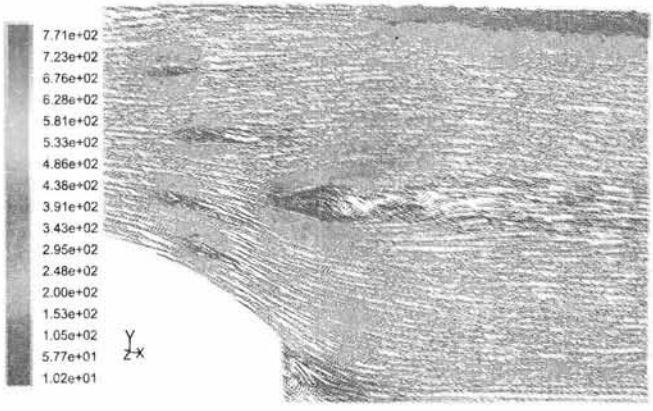

Fig. 15—Velocity (m/s) contours at a plane rotated 20° about x-axis from mid plane

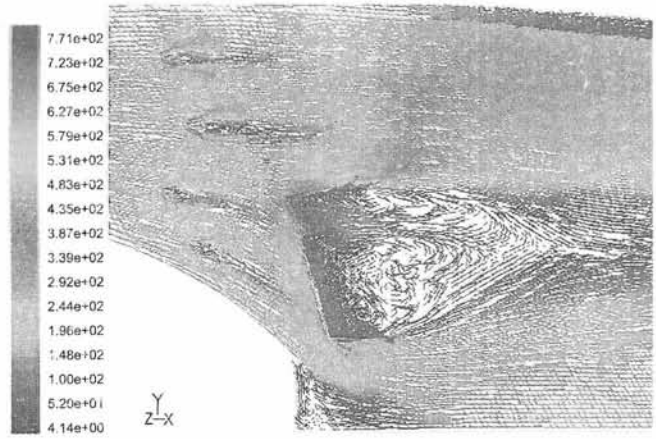

Fig. 16—Velocity (m/s) contours at a plane rotated 30° about x-axis from mid plane

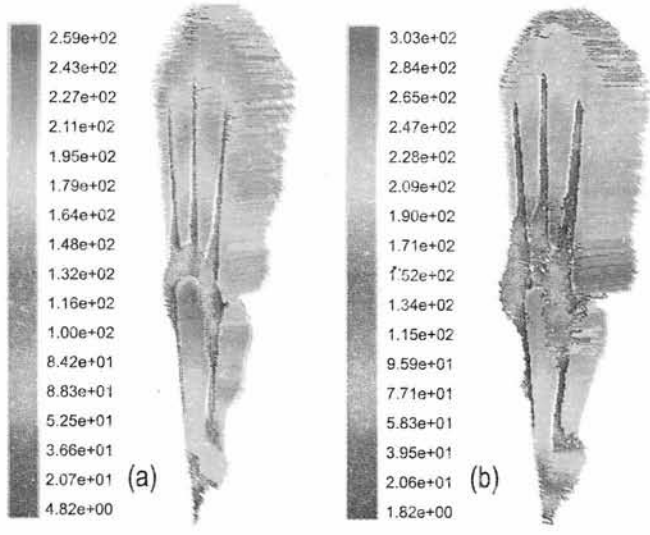

Fig. 17—Velocity (m/s) contours at cross-sectional planes [(a) 477.9 mm from core inlet and(b) 478.15 mm from core inlet]

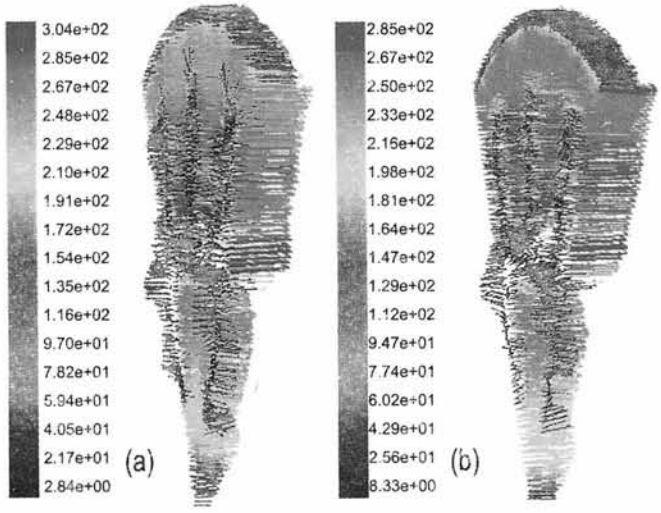

Fig. 18—Velocity (m/s) contours at cross-sectional planes [(a) 478.4 mm from core inlet and (b) 478.65 mm from core inlet]

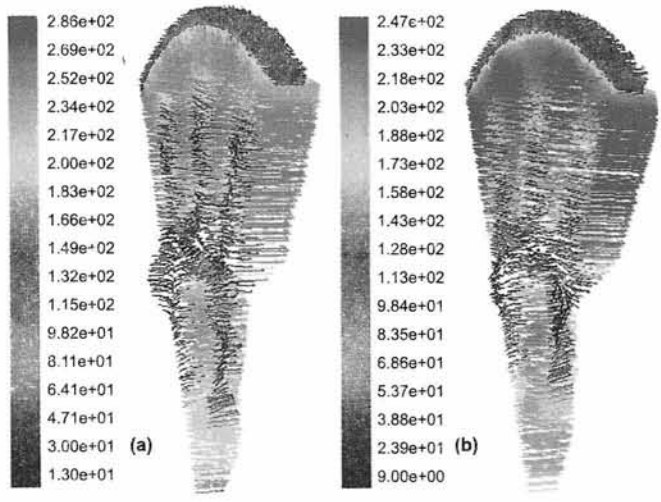

Fig. 19—Velocity (m/s) contours at cross-sectional planes [(a) 478.9 mm from core inlet and (b) 479.15 mm from core inlet]

Table 2—Mass flow rates at various sections and total pressure loss

Bypass inlet (kg/s)	Core inlet (kg/s)	Anti-screech rings (kg/s)	Cooling rings (kg/s)	Bypass exit (kg/s)	Pressure loss (%)
2.2	15	0.80841064 (36.74%)	0.289440238 (13.16%)	1.1015561 (50.0707%)	13.28931

Table 3—Thermodynamic and flow properties at inlet and outlet

	Velocity (m/s)	Mach number	Static pressure (Pa)	Total pressure (Pa)	Static temperature (K)	Total temperature (K)	Density (kg/m^3)	
Bypass Inlet	102.45522	0.14643542	327572.13	324463.81	592.40918	584.40918	2.6740344	
Core Inlet	278.31073	0.42487511	232089.72	280404.94	998.66345	1031.5972	1.2081925	
Nozzle Outlet	689.7085	1.3345232	12478.756	229675.63	724.11517	981.82526	0.54961741	

Figures 17-19 show velocity vectors at cross-sectional planes at indicated distances from the core inlet. Fig. 17 a shows a plane that bisects the gutter and five planes at equal intervals of 0.025 m have been presented in the figures. The important contribution of the ring gutter is seen in Fig. 17a in that the recirculation first sets-up in the lee of the ring gutter. As seen in Fig. 17b, the recirculation zone then spreads upwards and downwards through the top and bottom radial gutters respectively. The flow between the gutters accelerates due to the blockage offered by the gutters. This leads to clear separation of the recirculation zone and creation of the shear layers.

In Fig. 18a the recirculation zone is fully developed in the entire lee region exhibits flow separation from the surrounding flow field. In subsequent figures the strength of the recirculation zone is seen to be waning. At a distance of 479.15 mm from the core inlet the recirculation zone almost ceases to exist and the flow diffusion starts as evidenced by the lower maximum velocity magnitude at that plane as against at other planes upstream. It is suggested that such plots could be a crude form of estimating the size of recirculation zones which could aid in the design of the V-gutter, position optimization and also the fuel injection point and spray characteristics. The results of present study are tabulated in Tables 2 and 3.

The validation of the predicted flow fields has not been carried out but the results have been compared with existing results of Ravichandran and Ganesan[5,9] and are found to be in close agreement.

Conclusions

The three-dimensional computational model of a typical aircraft gas turbine engine afterburner incorporating all the complexities has been created

using GAMBIT preprocessor and the governing physical equations have been solved by the finite volume approach using FLUENT 6 solver. The predicted flow fields indicate the formation of individual recirculation zone in the lee of the top and bottom radial gutters as well as the ring gutter. The length of the recirculation zone downstream of the top radial gutter is more than that formed downstream of the bottom radial gutter. The recirculation zone is characterized by low velocities, which would aid in the formation of a region of low reaction rate and near adiabatic flame temperature and act as the continuous ignition source. The region of dissipation of the recirculation zone in the surrounding flow field indicates the formation of requisite shear layers, which would aid in the sustenance and completion of combustion. The diffuser performance is satisfactory and the Mach number is reduced from a value of 0.4248 at inlet to about 0.28 just upstream of the V-gutter. The nozzle performance is satisfactory and the exit Mach number is 1.334. However, the throat area of the nozzle is seen to contribute to avoidable pressure loss, which could be obviated by better design of the throat area. The pressure loss is 13.23% as measured from core inlet to nozzle outlet and 6.04% as measured from core inlet to nozzle inlet. The mass flow rates through cooling ring, anti-screech ring and bypass exit are in line with design intent.

References

1 James W Useller, *Effect of Combustor Length on Afterburner Combustion, Lewis Research center- NASA*, 1959.

2 Edwards J L, *J Royal Aero Soc*, 59 (530) (1955) 127-150.

3 Kumar R K, *Combust Sci Technol*, 21 (1980) 199-203.

4 Ganesan V, *Indian J Technol*, 18 (1980) 447-450.

5 Ravichandran M & Ganesan V, *Indian J Engg & Mater Sci*, 1 (1994) 309-319.

6 Lee D & Lin J S, *Numerical Heat Transfer*, Part A, 20 (1991) 65-79.

7 Ravichandran M & Ganesan V, *IE (I) J-MC*, 77 (1996) 67-75.

8 Frolov S M, Basevich V, Ya & Belyaev A A, " *Modelling of Bluff-Body Stabilized Combustion with Detailed Chemistry*", N.N.Semenov Institute of Chemical Physics, Moscow, 1999.

9 Ravichandran M & Ganesan V, *Int J Experiments Fluids*, 17 (1994) 59-67.

10 Ravichandran M & Ganesan V, *Int J Numerical Methods Heat Fluid Flow*, 6 (1996) 19-34.

11 FLUENT 5, *User's Guide Vol 2 and 3*, Fluent Inc. 1998.

12 Versteeg H K & Malalasekera W, *An Introduction to Computational Fluid dynamics The Finite Volume Method* (Longman Group Ltd), 1995.